JGR Atmospheres

RESEARCH ARTICLE
10.1029/2018JD030100

Regional Widening of Tropical Overturning: Forced Change, Natural Variability, and Recent Trends

Paul W. Staten[1], **Kevin M. Grise**[2], **Sean M. Davis**[3], **Kristopher Karnauskas**[4], **and Nicholas Davis**[3]

[1]Department of Earth and Atmospheric Sciences, Indiana University, Bloomington, IN, USA, [2]Department of Environmental Sciences, University of Virginia, Charlottesville, VA, USA, [3]NOAA Earth Systems Research Laboratory, Boulder, CO, USA, [4]Oceans and Climate Lab, University of Colorado Boulder, Boulder, CO, USA

Abstract The width of the tropical Hadley circulation (HC) has garnered intense interest in recent decades, owing to the emerging evidence for its expansion in observations and models and to the anticipated impacts on surface climate in its descending branches. To better clarify the causes and impacts of tropical widening, this work generalizes the zonal mean HC to the regional level by defining meridional overturning cells (RC) using the horizontally divergent wind. The edges of the RC are more closely connected to surface hydroclimate than more traditional metrics of regional tropical width (such as the sea level pressure ridge) or even than the zonal mean HC. Simulations reveal a robust weakening of the RC in response to greenhouse gas increases, along with a widening of the RC in some regions. For example, simulated widening of the zonal mean HC in the Southern Hemisphere appears to arise in large part from regional overturning anomalies over the Eastern Pacific, where there is no clear RC. Unforced interannual variability in the position of the zonal mean HC edge is associated with a more general regional widening. These distinct regional signatures suggest that the RCs may be well suited for the attribution of observed circulation trends. The spatial pattern of regional meridional overturning trends in reanalyses corresponds more closely to the pattern associated with unforced interannual variability than to the pattern associated with CO_2 forcing, suggesting a large contribution of natural variability to the recent observed tropical widening trends.

Plain Language Summary The large-scale tropical wind patterns responsible for the dry desert belts on either side of the tropics appear to be expanding. Most explanations for this widening are based on the tropics as a whole and do little to address whether the subtropics are widening from one region to the next. This study extends the definition of tropical width—specifically the Hadley cell edge—to the regional level. The regional tropical edge lines up with deserts better than another, more conventional regional indicator. The observed pattern of tropical widening more closely resembles natural changes than human-caused widening during much of the year.

Key Points:
- The local tropical edge diagnostic follows spatial hydroclimate variations more closely than does the subtropical ridge
- Observed widening, forced widening, and interannual variations each have their own regional signature
- The pattern of observed regional widening more closely matches unforced interannual variations than forced regional widening

Supporting Information:
- Supporting Information S1

Correspondence to:
P. W. Staten,
pwstaten@indiana.edu

Citation:
Staten, P. W., Grise, K. M., Davis, S. M., Karnauskas, K., & Davis, N. (2019). Regional widening of tropical overturning: Forced change, natural variability, and recent trends. *Journal of Geophysical Research: Atmospheres*, *124*, 6104–6119. https://doi.org/10.1029/2018JD030100

Received 4 DEC 2018
Accepted 1 MAY 2019
Accepted article online 17 MAY 2019
Published online 20 JUN 2019

Author Contributions:
Conceptualization: Paul W. Staten, Kevin M. Grise, Kristopher Karnauskas
Formal analysis: Paul W. Staten, Kevin M. Grise, Sean M. Davis, Nicholas Davis
Investigation: Paul W. Staten, Kristopher Karnauskas
Methodology: Paul W. Staten, Kevin M. Grise, Sean M. Davis, Nicholas Davis
Project administration: Paul W. Staten
Software: Paul W. Staten
Writing - original draft: Paul W. Staten
Writing – review & editing: Paul W. Staten, Kevin M. Grise, Sean M. Davis, Nicholas Davis

1. Introduction

The climate in the tropics and subtropics is often described as being dominated by the meridional overturning Hadley circulation (HC). The HC is observed to be widening by about 0.2° per decade in each hemisphere since 1979 (S. M. Davis & Rosenlof, 2012; Fu et al., 2006; Grise et al., 2019; Y. Hu & Fu, 2007; Seidel & Randel, 2007; Seidel et al., 2008; Staten et al., 2018), and both theory and models suggest that this widening will continue during the coming century as a result of continued greenhouse gas (GHG) concentration increases (Chen et al., 2008; D'Agostino & Lionello, 2017; Kim et al., 2017; Min & Son, 2013; Nguyen et al., 2015; Staten et al., 2012; Waugh et al., 2018). With over 1 billion people (~17% of Earth's human population) living within ±3° of the present HC edges (Doxsey-Whitfield et al., 2015), diagnosing the underlying circulation dynamics associated with recent projections of subtropical aridification (Cook et al., 2014; Karnauskas et al., 2016, 2018; Scheff & Frierson, 2015) is a timely challenge. However, the poleward shift of the edges of the tropical meridional overturning circulation is unlikely to occur at all longitudes around the world (Nguyen et al., 2017). Thus, a poleward shift of the HC edge does not guarantee a meaningful climate shift (such as aridification) in populated areas. While the HC is traditionally defined in the zonal mean for dynamical studies, the pressing question for societal impacts concerns the changes in the regional tropical meridional overturning circulation (RC).

A metric for the RC may help to distinguish the impacts of the many drivers of HC widening, each having their own seasonality and geography. Both stratospheric ozone (O_3) depletion and increasing GHG

concentrations shift the Southern Hemisphere (SH) tropical edge poleward, with the ozone influence maximining in austral summer (December–February, DJF) and the greenhouse gas influence maximizing in austral summer and fall (March–May, MAM; D'Agostino & Lionello, 2017; N A Davis et al., 2016; McLandress et al., 2010; Min & Son, 2013; Nguyen et al., 2012; Polvani et al., 2010; Son et al., 2010; Staten et al., 2012; Stocker et al., 2013). Tropospheric pollutants, including black carbon, ozone, and sulfate aerosols, have a distinct geography owing particularly to recent rapid development in Eastern and Southeastern Asia but also to reductions in pollutions over other developed nations (Allen & Ajoku, 2016; Allen et al., 2012; Kovilakam & Mahajan, 2016). Changes in heat transport by the ocean similarly drive changes in tropical atmospheric overturning, across a range of temporal and spatial scales (Schneider et al., 2014). Coupled atmosphere-ocean variability (e.g., the El Niño–Southern Oscillation, or ENSO, the Pacific Decadal Oscillation) is known to drive multidecadal variability in the tropical overturning circulation (Allen & Kovilakam, 2017; Amaya et al., 2017; Feng, Li, Kucharski, et al., 2018; Feng, Li, Jin, Zhao, et al., 2018; Feng, Li, Jin, & Zheng, 2018; Feng et al., 2012; Grassi et al., 2011; Guo et al., 2016; Li et al., 2004; Mantsis et al., 2017; Quan et al., 2014; Stanfield et al., 2016). Even internal atmospheric variability appears to play an important role in the width of the HC on multidecadal timescales (Garfinkel et al., 2015; Simpson, 2018).

Traditional methods for defining the regional extent of the tropics include outgoing longwave radiation thresholds, sea level pressure (SLP) maxima, and tropopause-based metrics. But outgoing longwave radiation is affected not only by changes in the tropical circulation but also by thermodynamic changes and is thus a poor measure of variability and change in the tropical overturning circulation, at least in the zonal mean (Waugh et al., 2018). The SLP changes associated with the HC are strongest over oceans (Schmidt & Grise, 2017), even though the tropical overturning circulation has clear impacts over both land and ocean (Chen et al., 2014; Freitas et al., 2017; Huang et al., 2018; Lucas & Nguyen, 2015; Zhao & Moore, 2008). For example, all of the world's hot deserts occur in or near subtropics. Tropopause-based metrics (Lucas et al., 2012; Lucas & Nguyen, 2015; Mathew & Kumar, 2018) tend to coincide with the subtropical jet more than with surface climate. Manney and Hegglin (2018) and Totz et al. (2018) examine jet separation, but aside from occasional ambiguity between the subtropical and extratropical jet, the latitudes of the subtropical jets more closely coincide with upper level dynamics than surface hydroclimate. Even in the zonal mean, many metrics based on the subtropical jet or tropopause are poorly correlated from year to year with the width of the HC (N. Davis & Birner, 2017; Nick A. Davis et al., 2018; Staten et al., 2018; Waugh et al., 2018).

The impacts of tropical overturning on surface climate motivate the use of a different metric. The HC drives precipitation in the deep tropics through ascent and convergence of water vapor and suppresses precipitation in the subtropics through descent and divergence of water vapor. Continuity guarantees a horizontal flow that links the subsidence and the divergence. The circulation over the subtropics, then, is of particular interest inasmuch as it creates low-level divergence. Specifically, much of the vertical motion in the tropics and subtropics (Figure 1a) is due to meridional divergence (Figure 1b), although zonal divergence also plays an important role near coastlines and in midlatitudes (Figure 1c).

Schwendike et al. (2014) use this same decomposition to examine belts of ascent and descent related to meridional and zonal overturning in the climatology and how they vary with ENSO. Schwendike et al. (2015) further highlight trends in the strength of the vertical mass flux associated with meridional overturning, noting a southward shift of the descent over Africa and a strengthening over the Americas and the Atlantic but stopping short of defining an RC edge. Nguyen et al. (2017; hereafter NG17) calculate an RC edge but average the divergent wind in the ERA-Interim reanalysis over roughly one third of the tropical belt at a time, citing variations in the strength of the Walker circulation in the countervailing variations of the zonal mean and Australian cells versus the South American and African cells. In the present study, we analyze forced, unforced, and observed changes of this thermally direct overturning circulation (RC) at all longitudes.

The rest of this paper is organized as follows. In section 2, we document the data sources utilized in this study, as well as the calculation and validation of the RC. In section 3, we examine the CO_2-forced changes of the RC (section 3.1). We then document unforced variations in the RC (section 3.2) and compare the forced and unforced variations to recent trends in two reanalyses (section 3.3). We finish by discussing the implications of our work (section 4).

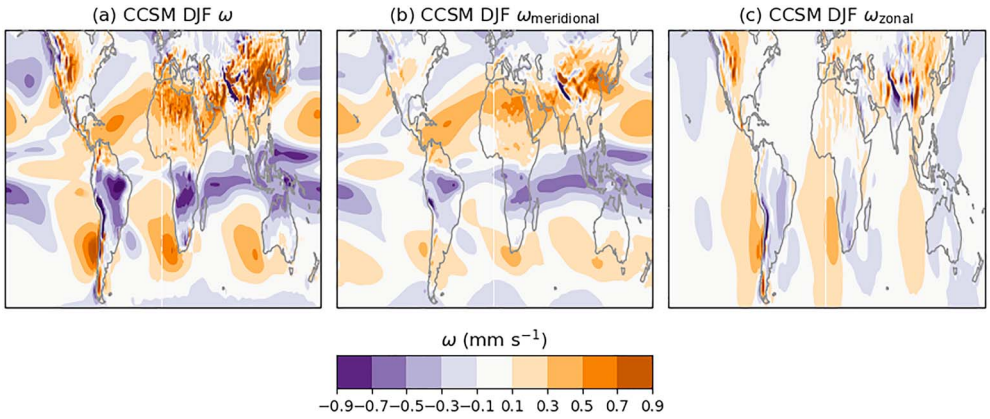

Figure 1. The (a) pressure velocity ω at 500 hPa calculated kinematically from the divergent wind and its additive components (b) $\omega_{meridional}$, derived from the meridional component of the divergent wind, and (c) ω_{zonal}, derived from the zonal component of the divergent wind, using data from the fully coupled CESM1.0 piControl simulation during DJF. Note that results in this study are calculated from the meridional component of the divergent wind not from the entire meridional wind. DJF = December–February.

2. Data and Methods

2.1. Model and Reanalysis Data

This study makes use of a combination of gridded temperature, horizontal wind, SLP, surface pressure, precipitation, and evaporation data from general circulation models and two modern reanalyses.

2.1.1. The CMIP5 Multimodel Ensemble

To examine the forced response (section 3.1), we use a multimodel average drawn from the Coupled Model Intercomparison Project phase 5 (CMIP5; Taylor et al., 2011) to reduce the sensitivity to the choice of model. We investigate forced changes due to greenhouse gas concentration increases by comparing the multimodel mean difference between preindustrial control (piControl) and quadrupled CO_2 (abrupt4 × CO_2) experiments. The piControl and abrupt4 × CO_2 experiments have the same initial conditions and forcings, with one important exception; the abrupt4 × CO_2 experiments have 4 times the preindustrial concentrations of well-mixed greenhouse gases prescribed from the first day of the model integration, while the piControl experiments retain preindustrial concentrations. The abrupt4 × CO_2 simulations are integrated for 150 years from the time that greenhouse gases are abruptly quadrupled from their preindustrial levels, but in order to allow the general circulation time to equilibrate prior to averaging (Ceppi et al., 2018; Grise & Polvani, 2017), we base our abrupt4 × CO_2 climatologies on the last 50 years of each simulation in order to better represent the equilibrium response, following Grise and Polvani (2016). The requirement that each model has dynamical variables archived during all 150 years of their respective integrations limits us to 23 models: ACCESS1.0, BCC-CSM1.1, BCC-CSM1.1(m), CCSM4, CNRM-CM5, CSIRO-Mk3.6.0, CanESM2, FGOALS-s2, GFDL-CM3, GFDL-ESM 2G, GFDL-ESM 2M, GISS-E2-H, GISS-E2-R, HadGEM2-ES, INMCM4, IPSL-CM5A-LR, IPSL-CM5B-LR, MIROC-ESM, MIROC5, MPI-ESM-LR, MPI-ESM-P, MRI-CGCM3, and NorESM1-M.

2.1.2. The CESM Large Ensemble

To examine natural year-to-year variability, we make use of three controls runs conducted as part of the Community Earth System Model (CESM) Large Ensemble (LE) project (Kay et al., 2014). We perform regressions using years 400–2,200 of a 2,200-year fully coupled atmosphere-ocean control simulation, years 1–1,000 of a 1,000-year slab-ocean control simulation, and years 1–1,600 of a 1,600-year-prescribed sea surface temperature experiment.

2.1.3. Reanalyses

To examine recent historical changes in tropical width, we make use of two reanalyses: ERA-Interim (Dee et al., 2011) and MERRA2 (Bosilovich et al., 2015; Gelaro et al., 2017). We make use of the full available timespan for each—1979–2017 for ERA-Interim and 1980–2017 for MERRA2.

2.2. The Helmholtz Decomposition

To apply the Helmholtz decomposition (Keyser et al., 1989; Schwendike et al., 2014), we calculate the overturning stream function at each longitude as $\Psi_\phi = \frac{1}{g}\int_0^p v_d dp$, where v_d is the meridional component of the

divergent wind only. Here *dp* is calculated as the pressure at each level minus the pressure of the level above (or minus zero in the case of the topmost pressure level).

Note that integrating Ψ_ϕ zonally recovers the conventional zonal mean mass stream function Ψ (depicted in Figures 2b and 2d). In calculating Ψ_ϕ, we filter out horizontal rotational wind features, including those that produce enhanced Hadley cell-wise flow—but no vertical motion—along the west coasts of North America, South America, Africa, and Australia (see Figures 2c, 2d, 2g, and 2h of Karnauskas & Ummenhofer, 2014). We examine the RC intensity and width by mapping the Ψ_ϕ field at 500 hPa level (hereafter $\Psi_{\phi,500}$). One disadvantage to the Helmholtz decomposition is that it necessarily aliases diagonally oriented (e.g., southwest to northeast) circulations onto a pair of zonal and meridional circulations. Despite this drawback, even diagonal bands of ascent and descent (like those over the northeast Pacific in Figure 1) are well reproduced (albeit of smaller magnitude) by the meridional wind. A more complete decomposition of the 3-D flow field, which further separates the Rossby wave component, is also possible, but the simple Helmholtz decomposition yields very similar results (S. Hu et al., 2017).

To calculate useful boundaries of the tropics, we simply mark the meridional zero crossings of the $\Psi_{\phi,500}$ field (contours in Figure 2). Specifically, we mark any negative-to-positive (south to north) zero crossings between 20 °S and 20 °N as RC-intertropical convergence zone (ITCZs) and any positive-to-negative (south to north) edges between 15° and 45° in each respective hemisphere as RC edges. The choice of latitudinal limits was practical; the overlap between the RC-ITCZ domain and the RC edge domain was chosen to allow for narrow circulation cells near the deep tropics. The 45 °N-S limit for RC width filters out zero crossings in the extratropics, which are generally weak and very unlikely to be related to tropical overturning. Our method does not yield an RC-ITCZ or RC edges at every longitude (see Figure 2). Furthermore, this method allows for multiple RC edges to exist within the same hemisphere and longitude (see, e.g., the double RC edges where the ~25 °N Atlantic-to-West Asian RC edge and the ~40 °N East Asian RC edge overlap in Figure 2a). Throughout this paper, we refer to an RC as a region of $\Psi_{\phi,500}$ bounded by an RC-ITCZ in the tropics and an RC edge on its poleward flank (see the annotations in Figures 2a and 2c). The same procedure as outlined above, when applied to the one-dimensional Ψ_{500} field, can provide metrics for the zonal mean HC-ITCZ and HC edge. However, it is important to note that while the zonal integral of the $\Psi_{\phi,500}$ field yields the conventional Ψ_{500} field, the zonal mean of the regional metrics does not equal the metrics derived from zonal mean fields.

To test the sensitivity of our RC existence on the threshold chosen for its edge detection, we also calculate the latitude at which the $\Psi_{\phi,500}$ drops to 10% of its maximum value in the subtropics (circles in Figure 2). The choice between the zero crossing and the 10% crossing makes little difference at most longitudes and in most seasons. To compare our results to those of NG17, we also apply their weaker threshold of 25% over specific regions. But for most of this study, our regional analysis does not rely on a RC being defined at every longitude or time step, so we have no need to relax the zero-crossing requirement as in NG17.

We note that in all of our calculations, we calculate seasonal averages of the data before calculating the divergent wind field, the longitudinally varying meridional stream function, or the RC edges (Adam et al., 2018). Also, we perform our analysis for all four seasons; but for clarity and brevity, we show results for DJF and June–August (JJA) in the main text and corresponding results for MAM and September–November (SON) in the supporting information.

2.3. Validating the RC Edge

The value of any metric lies in its ability to quantify the physical phenomenon it is *intended* to measure. A metric for the edge of the tropics should (1) approximate fundamental measures such as SLP maxima and (2) coincide with extrema in precipitation minus evaporation. That is, if we argue that deserts cluster in the subtropics because of subsidence associated with the HC, then the RC should have edges near deserts.

To validate the RC edge metric, we compare the RC edge and $\Psi_{\phi,500}$ field with the SLP and precipitation-minus-evaporation (P-E) fields calculated from preindustrial control simulation output produced using CESM1.0 (Figure 3). In the zonal mean, the HC edge (Figures 3c and 3f, black circles) and the subtropical SLP maxima (Figures 3c and 3f, red squares) are closely collocated, but the regional SLP maxima are generally poleward of their corresponding RC edges (Figures 3a and 3d; compare the red shading to the horizontal dashes).

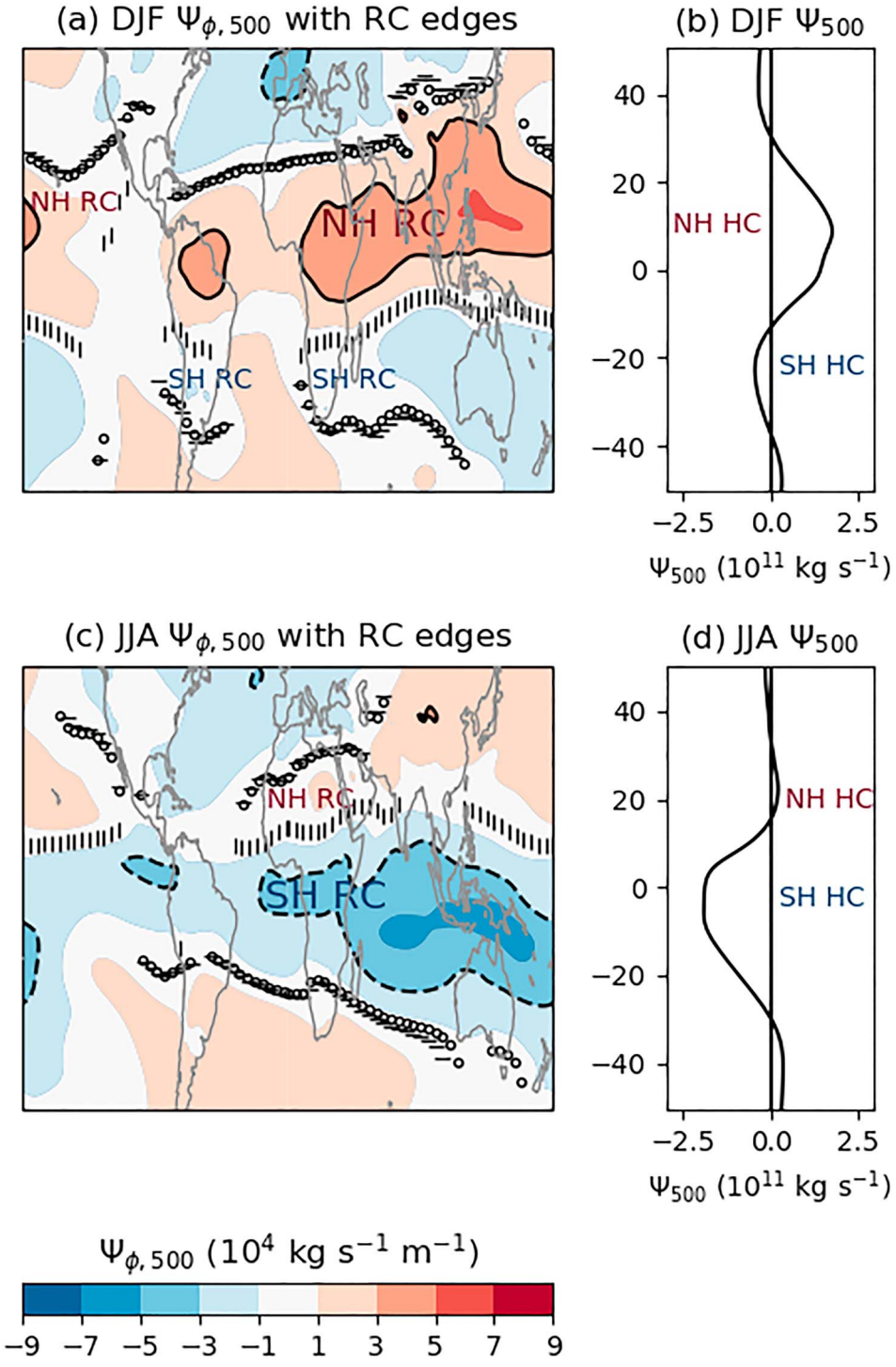

Figure 2. The 500-hPa meridional stream function $\Psi_{\phi,500}$ (shading, with black contours at $\pm 3 \times 10^4$ kg s^{-1} m^{-1} for reference with later figures) at each longitude (a, c), along with the traditional Ψ_{500} (b, d) during DJF (a, b) and JJA (c, d), from the fully coupled CESM1.0 piControl experiment. Poleward RC edges (the regional extension of the HC edge) are shown using horizontal dashes, while the RC-ITCZ is shown using vertical dashes. The 90% drop on either side of the RC maxima (an alternative metric for the RC edge) is shown in black circles. DJF = December–February; JJA = June–August.

In Northern Hemisphere (NH) winter (Figure 3a), the subtropical ridge and the RC edge are defined at most longitudes, but in NH summer (Figure 3d) and in the SH, regional SLP maxima are concentrated into "centers of action" (Angell et al., 1969). These centers of action tend to occur over the ocean and at longitudes

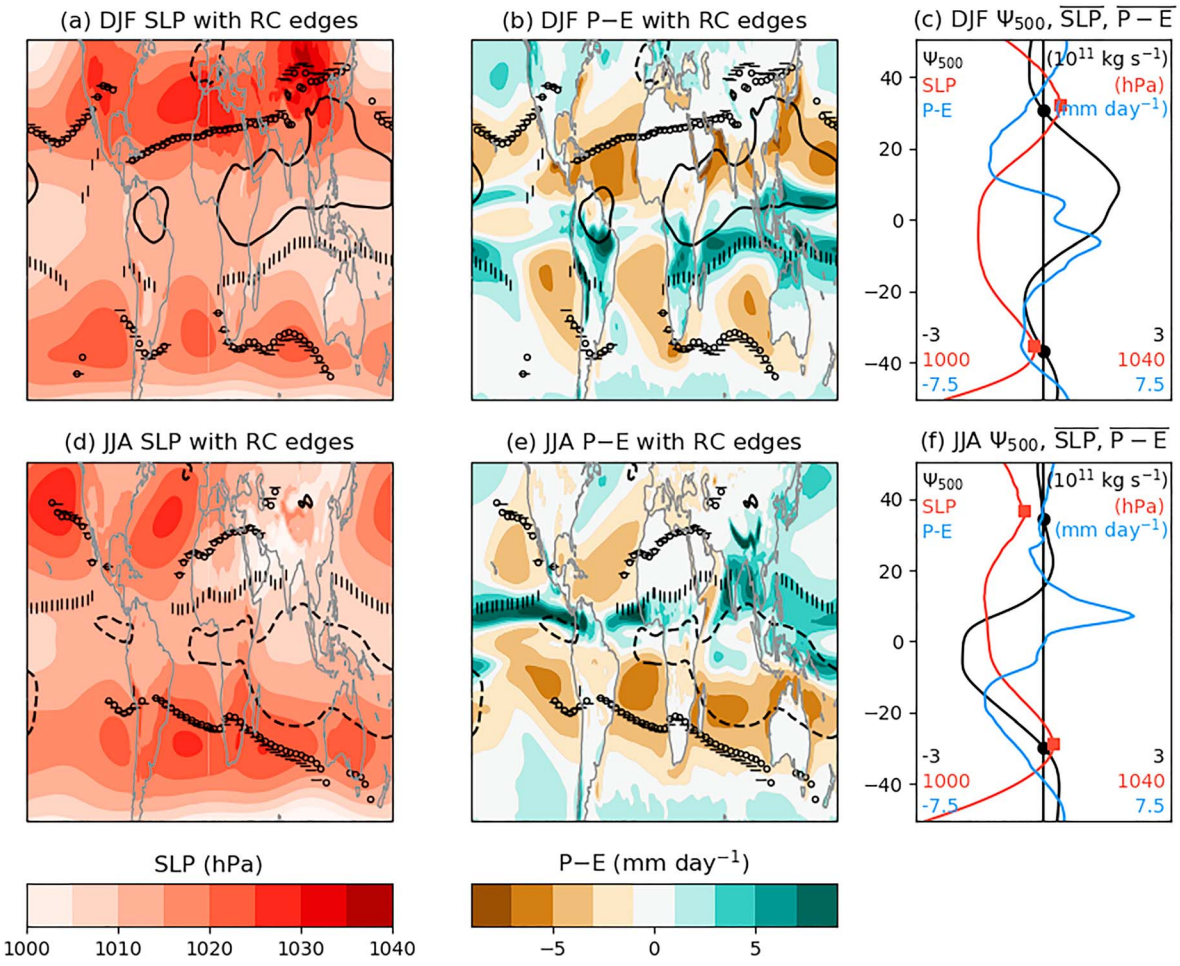

Figure 3. RC edges (horizontal dashes), the RC-ITCZ (vertical dashes), and $\Psi_{\phi,500}$ strength (contours at $\pm 3 \times 10^4$ kg s^{-1} m^{-1} taken from Figure 2) in the context of (a, d) SLP (shaded) and (b, e) P-E (shaded). Also shown are the corresponding zonal mean fields (c, f; color coded with labels and units marked on top and ranges marked on bottom). Data come from the fully coupled CESM1.0 piControl simulation. The 90% $\Psi_{\phi,500}$ cutoff is shown in hollow circles in (a, b, d, and e). DJF = December–February; JJA = June–August; P-E = precipitation-minus-evaporation; SLsea level pressure.

where the RC is weaker, particularly in the summer hemispheres (SH DJF in Figure 3a and NH JJA in Figure 3d). Summarizing, while regional SLP maxima such as the North Atlantic and North Pacific subtropical highs are best defined during the summer (Hoskins, 1996; Song et al., 2018), the RC is best defined during the winter. The RC edge is also well defined during the equinox seasons over both hemispheres (Figure S1) and tends to skirt the equatorward flanks of the subtropical SLP maxima (Figure S2).

Compared to the SLP maxima, the poleward RC edges more closely follow the latitudes of P-E minima associated with the dry subtropics over both hemispheres (Figures 3b and 3e) and during all four seasons (Figures 3 and S2). Where the RC edges are clearly defined, they generally lie at or just poleward of the subtropical P-E minima. Conversely, where a strong P-E minimum exists, an RC edge and associated descent is found nearby. Over land, the poleward RC edges correspond closely to regions of climatologically dry surface climate, that is, to hot deserts. For example, the RC edge tracks through the Saharan and Arabian deserts, even though the driver for the subsidence in these regions may be a Rossby wave forced by diabatic heating in Asian monsoon region (Rodwell & Hoskins, 1996), rather than a Lagrangian overturning loop between the equator and subtropics. Also, in contrast to the SLP field, $\Psi_{\phi,500}$ clearly delineates an RC-ITCZ which corresponds closely to the hydrological ITCZ, that is, the P-E maximum. Finally, the RC roughly delineates regions in which precipitation is dominated by the mean overturning circulation, rather than by eddies (see Figure 3 in Seager et al., 2010).

Some relationships between zonal mean metrics are even clearer in our regional analysis. The P-E minimum equatorward of the HC edge (Figures 3c and 3f) is even sharper at most longitudes, since there is no smearing due to zonal averaging. For example, while the HC is poorly defined during JJA over the NH, the RC over North Africa is well defined during that season and descends over the northern edge of the Sahara. Similarly, the tropical P-E maximum, which occurs on the wintertime side of the RC-ITCZ (Figures 3c and 3f) in the zonal mean, follows even more closely with the RC-ITCZ at most longitudes, suggesting that energetic arguments considering the ITCZ to be an energy-flux equator (e.g., Kang et al., 2008) are valid even at a regional level.

3. Results

3.1. Forced RC Change in CMIP5 Models

While greenhouse gas concentration increases are expected to widen the zonal mean HC, this does not necessarily imply that they will widen the RC everywhere—or even *any*where. For example, a shift in the HC edge may result from a regional trend in $\Psi_{\phi,500}$ at a longitude where no RC exists. Furthermore, the zonal mean HC by construction cannot capture a zonal shift of an RC.

The $4 \times CO_2$ response of the $\Psi_{\phi,500}$ field in CMIP5 (Figures 4a, 4e, S3a, and S3e) includes a weakening of both the summertime and wintertime RCs at most longitudes (cool shading in the NH RC and warm shading in the SH RC), consistent with the zonal mean HC weakening (Figures 4b, 4f, S3b, and S3f; Betts, 1998; Feldl & Bordoni, 2015; Held & Soden, 2006; Schneider et al., 2010; Vecchi & Soden, 2007). But the weakening of the RC is even stronger than the weakening of the zonal mean HC (after dividing the latter by the circumference of the earth) because the zonal average includes cancelling contributions from both a weakening RC and a weakening thermally indirect circulation over the South Atlantic (during DJF) and the Eastern Pacific (blue shading over the said regions in Figure 4a).

Previously, an anticorrelation between HC width and strength has been noted in response to the seasonal cycle (Nguyen et al., 2012), during El Niño and La Niña events (Lu et al., 2008), in paleoclimate simulations (D'Agostino, Lionello, Adam, et al., 2017) and in idealized experiments with prescribed tropical heating (Chang, 1995), but it has not as yet been explained mechanistically. Furthermore, we show here that at a regional level, this anticorrelation does not strictly hold, but that the widening of the RC (shading at the RC edges) is much more localized than the weakening (shading in the RC interiors; see Figures 4 and S3). The widening of the RC is thus a common but not definitive, accompaniment to RC weakening in response to increased GHG concentrations.

During DJF, a weak zonal mean poleward HC shift in the NH (Figure 4b) coincides with RC widening centered over the Middle East and the Western Pacific, but it also coincides with RC contraction over the American Southwest, the North Atlantic, and East Asia (Figure 4a). SH HC expansion is clearer in all four seasons (Figures 4b, 4f, S3b, and S3f), owing largely to significant negative $\Psi_{\phi,500}$ anomalies over the east Pacific, even though no climatological RC is defined in this region during JJA (Figure 4e), and only a weak RC exists during DJF (Figure 4a) and MAM (Figure S3a). NH mean widening during SON (Figure S3b) is dominated by positive $\Psi_{\phi,500}$ anomalies over the east Pacific and the Middle East.

The above results demonstrate that forced tropical widening may be more robust in a few regions (e.g., over South America) than the zonal mean HC would indicate. Furthermore, east-west shifts in the RC—which appear as north-south shifts when the RC edge is sloped—can be missed by the HC completely.

In contrast to the RC edge, the subtropical ridge (see Figures 4c, 4d, 4g, 4h, S3c, S3d, S3g, and S3h) shifts poleward almost uniformly over the SH year round in a warming climate, even at longitudes where no RC is defined (e.g., the South Central Pacific during JJA; Song et al., 2018); in some cases, the SLP signal may reflect changes in the eddy-driven jet rather than the RC (Pena-Ortiz et al., 2013). Our results suggest that caution should be exercised when interpreting the zonal mean SH climate change response; traditionally, the strong HC widening signal over the SH is ascribed in part to the reduced land-sea contrast over the SH and a more zonally symmetric circulation. But while the midlatitude circulation and subtropical ridge are certainly more zonal over the SH, the forced $\Psi_{\phi,500}$ anomalies associated with HC widening are dominated by the Eastern Pacific.

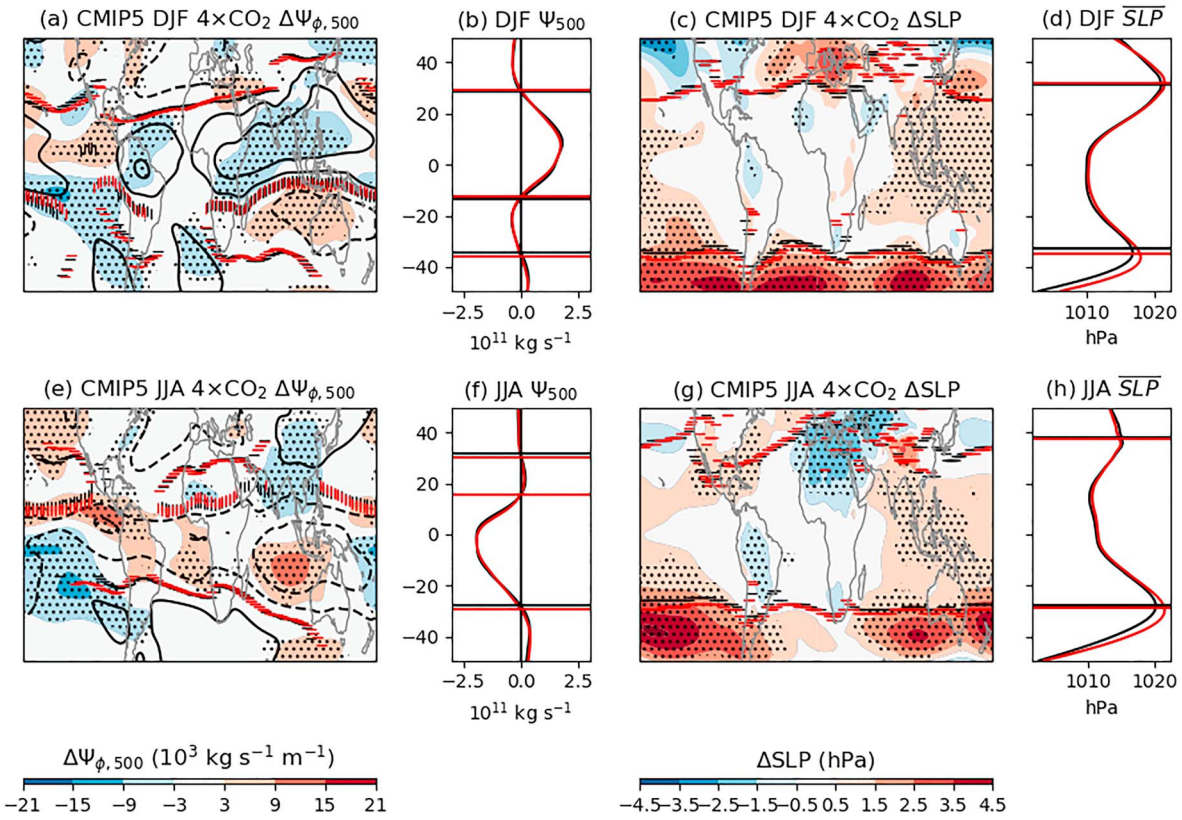

Figure 4. Forced changes in (a, e) $\Psi_{\phi,500}$ and the RC edges (horizontal and vertical dashes; piControl edges are black, and $4 \times CO_2$ are red) with climatological contours at $\pm(3,7) \times 10^4$ kg s^{-1} m^{-1}, (b, f) Ψ_{500}, (c, g) SLP and the subtropical high (horizontal dashes), and (d, h) $\overline{SLP}$ in response to a quadrupling of CO_2 in a CMIP5 multimodel ensemble during DJF (a–d) and JJA (e–h). Stippling indicates that at least 20 models indicate a change of the same sign. CMIP5 = Coupled Model Intercomparison Project phase 5; DJF = December–February; JJA = June–August; SLsea level pressure.

Over the North Pacific, the subtropical ridge and the RC edge shift equatorward during JJA, while the RC edge shifts poleward during DJF, consistent with the seasonality of the Pacific jet response (Grise & Polvani, 2014; Shaw & Voigt, 2016; Simpson et al., 2014).

3.2. Natural RC Variability in CESM

One overarching challenge in studying the widening of the tropics is discerning a forced response from natural variability. One approach is to analyze the spatial pattern of RC changes associated with forced and unforced HC variations. We know the HC widens in forced warming simulations; but does a widening HC in a forced simulation have similar impacts geographically as an unforced widening HC from one year to the next?

The changes in $\Psi_{\phi,500}$ and the RC edges due to unforced variations in the CESM control runs (Figures 5, 6, S4, and S5) contrast sharply with the forced response to quadrupling CO_2 in CMIP5 (Figures 4a, 4d, S3a, and S3d). Compared to their forced counterparts, unforced changes in $\Psi_{\phi,500}$ are smaller scale (regional scale rather than planetary scale) and peak at different longitudes. During DJF over the NH, forced RC widening occurs over the Sahara and Middle East and Central Pacific (Figure 4a), while unforced widening of the NH HC is focused near the Gulf of California (reminiscent of ENSO), Africa's Northwest coast, and the Himalayas (Figures 5a–5c). During JJA over the SH, forced RC widening occurs mainly due to a tendency toward thermally direct circulation over the South Pacific (Figure 4e), while unforced widening occurs near South America, Africa, and the Indian Ocean (Figures 6a–6c). Year round over the SH, CO_2 increases result in negative $\Psi_{\phi,500}$ anomalies in the subtropical Eastern Pacific (Figures 4a, 4e, S3a, and S3e), often contributing to a widening of the SH HC as mentioned in section 3.1, but natural coupled SH HC

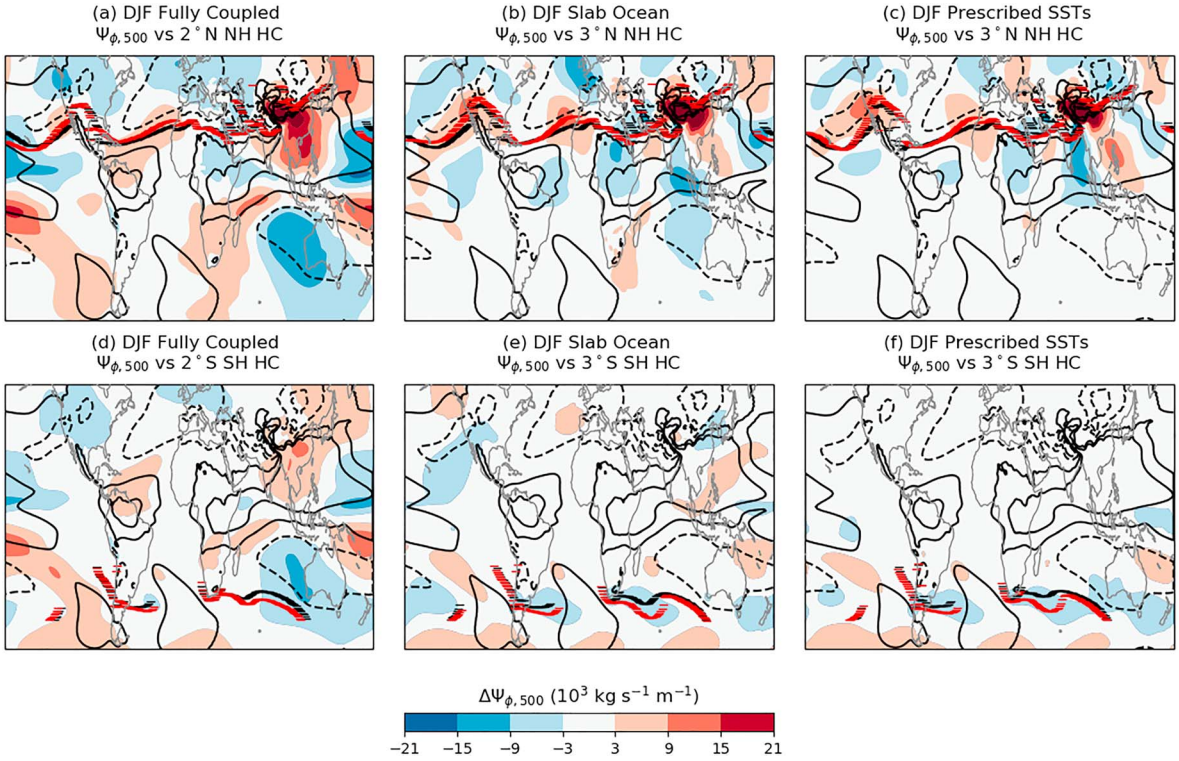

Figure 5. Regression of $\Psi_{\phi,500}$ onto unforced 2° poleward shifts (for fully coupled experiments) or 3° poleward shifts (for the slab ocean and prescribed SST experiments) of the zonal mean (a–c) NH HC and (d–f) SH HC from Community Earth System Model Large Ensemble during DJF. Climatological contours are shown at $\pm(3,7) \times 10^4$ kg s^{-1} m^{-1}. Black horizontal dashes indicate the climatological RC edge in the respective hemisphere, and red horizontal lines indicate the RC edge calculated from the climatology with the regressed $\Psi_{\phi,500}$ superimposed. The regressions are performed using output from (a, d) a fully coupled model, (b, e) a land-atmosphere model coupled to a slab ocean, and (c, f) a land-atmosphere model with prescribed SSTs. DJF = December–February; HC = Hadley circulation; NH = Northern Hemisphere; SH = Southern Hemisphere.

widening coincides with negative $\Psi_{\phi,500}$ anomalies over the Indian Ocean, often strengthening and widening the RC there (Figures 5d, 6d, S4d, and S5d).

A surprising result of this analysis is that year-to-year changes in the strength of the RC in each of the CESM LE control integrations—namely, the coupled atmosphere-ocean simulations (the left-most panels of Figures 5, 6, S4, and S5), the slab-ocean simulations (the center panels), and the atmosphere-only simulations (the right-most panels) —differ strongly, but the resulting variations in RC extent are quite

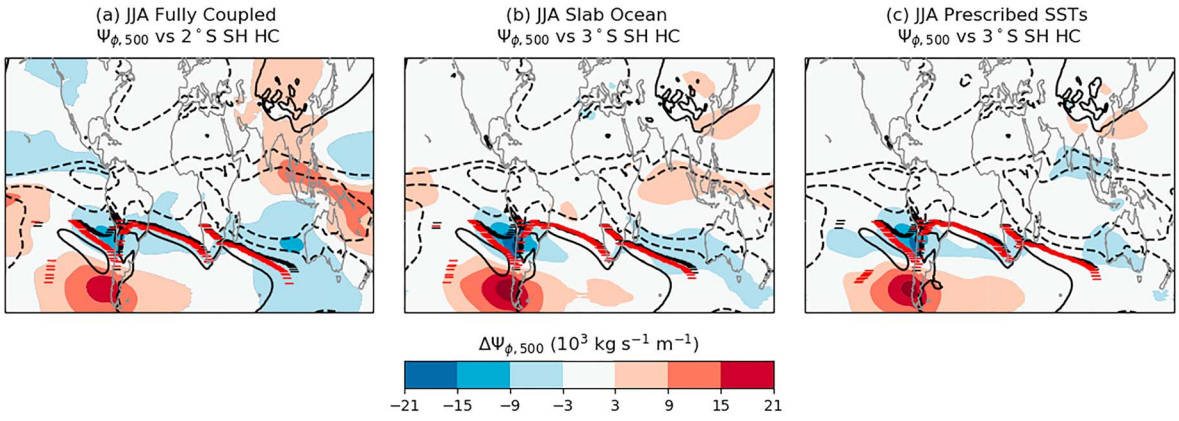

Figure 6. As for Figure 5 (d–f) but for JJA. (Only SH regressions are shown, as the zonal mean HC is poorly defined over the Northern Hemisphere during JJA.) JJA = June–August; HC = Hadley circulation; SH = Southern Hemisphere.

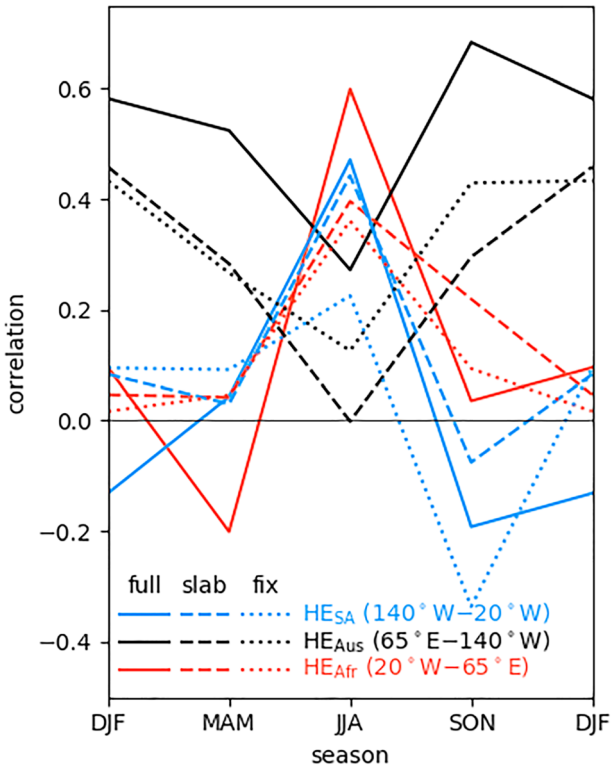

Figure 7. Interannual correlations between the zonal mean Southern Hemisphere Hadley circulation edge and the regional cells as in Fig. 4 of NG17 but for DJF, MAM, JJA, and SON. The hemispheric cells here are defined as in NG17 as the latitude where the $\Psi_{\phi,500}$, averaged over the respective latitude bands (HE_{Aus} = 65 °E – 140 °W, HE_{Afr} = 20 °W – 65 °E, HE_{SA} = 140 °W – 20 °W), reaches 25% of its maximum value nearer the equator. The line styles denote the Community Earth System Model experiment from which the correlations are calculated: "full" for fully coupled simulation, "slab" for the atmosphere model coupled to a slab ocean, and "fix" for the atmosphere-only model run with fixed SSTs. DJF = December–February; MAM = March–May; JJA = June–August; SON = September–November.

similar. Specifically, HC variations in the coupled simulation result from an anomalous overturning field distinct from that in dynamically uncoupled simulations, with the strongest differences near the Maritime Continent, the Western Pacific, Western North Atlantic (during DJF; Figures 5a and 5d) and South Atlantic (during JJA, Figure 6 a). The similarity of the regressions onto NH HC edge latitude (Figures 5a and S4a) and onto SH HC edge latitude (Figures 5d and S4d) during DJF and MAM elegantly illustrate hemispherically symmetric variability associated with coupled modes of variability such as El Niño (Seager et al., 2003); the uncoupled simulations show little such symmetry. The strengthening and widening of overturning is particularly intense in the Maritime Continent region, in agreement with the La Niña regression in Schwendike et al. (2014).

While the largest changes in RC intensity are absent in the slab ocean and prescribed SST simulations (the center and right panels in Figures 5, 6, S4, and S5), the anomalies in the immediate vicinity of the RC edge—and hence the widening of the RC—are very similar in all three control simulations. Assuming the leading modes of variability in the HC edge in the prescribed SST simulations are eddy driven, this would suggest that midlatitude eddies are key modulators of the RC width in both coupled and uncoupled scenarios (Kang et al., 2013). Our analysis does not determine whether the changing RC width modifies the eddy flux (Mbengue & Schneider, 2018) or whether the midlatitude eddies change RC width, but it suggests that extratropical variability may drive similar changes in HC width in both coupled and uncoupled experiments alike. When considering mechanisms of poleward expansion, then one may need to consider not just the local diffusivity to eddies (set in part by conditions in the tropics) but also eddy generation and flux from the extratropics (Staten et al., 2014).

3.2.1. Our Interannual Regressions Versus NG17

While our regressions show a wide RC over South America during years with a wide HC, NG17 finds a negative correlation between the latitudes of South American Hadley Cell (HE_{SA}) edge and the zonal mean edge in the ERA-Interim reanalysis. The difference is due primarily to the choice of longitude band 140–20 °W represented by HE_{SA} in NG17. This range includes the Southeast Pacific, where a large swath of positive $\Psi_{\phi,500}$ anomalies (Figure 5d) act to contract the RC edge during years when the zonal mean HC is further poleward.

NG17 attributes the anticorrelation between the HE_{SA} width and the SH HC width to a Gill-type response to heating over the Maritime continent and in particular to variations in the strength of the Walker circulation. By replicating their results for the coupled and uncoupled CESM LE (see Figure 7 compared to Figure 4 from NG17), we qualify the importance of ENSO and surface heating to the regional HC width. As in NG17, we confirm the negative correlation between the width of HE_{SA} and the SH HC during SON and DJF (Figure 7, solid blue line) and the near-zero correlation between the South African Hadley cell (HE_{Afr}) edge and the SH HC during the same months (Figure 7, solid red line). During most seasons, the correlations between the regional cell edges and the zonal mean cell generally decrease without a coupled ocean; we posit that RC width variations become less organized, rather than being preferentially dominated by shifts from one region or another. But it is interesting to note that while the correlation between HE_{SA} and the zonal mean HC changes is weakly positive during DJF for the slab ocean and fixed-SST experiments (Figure 7, blue dashed and blue dotted lines), the seasonal cycle is broadly similar, and the negative SON correlation is even stronger in the fixed SST experiment. Thus, while coupled ENSO variations and a Gill-type response may indeed be responsible for the correlations in the observed data record, they may not be necessary to produce the seasonality observed by NG17.

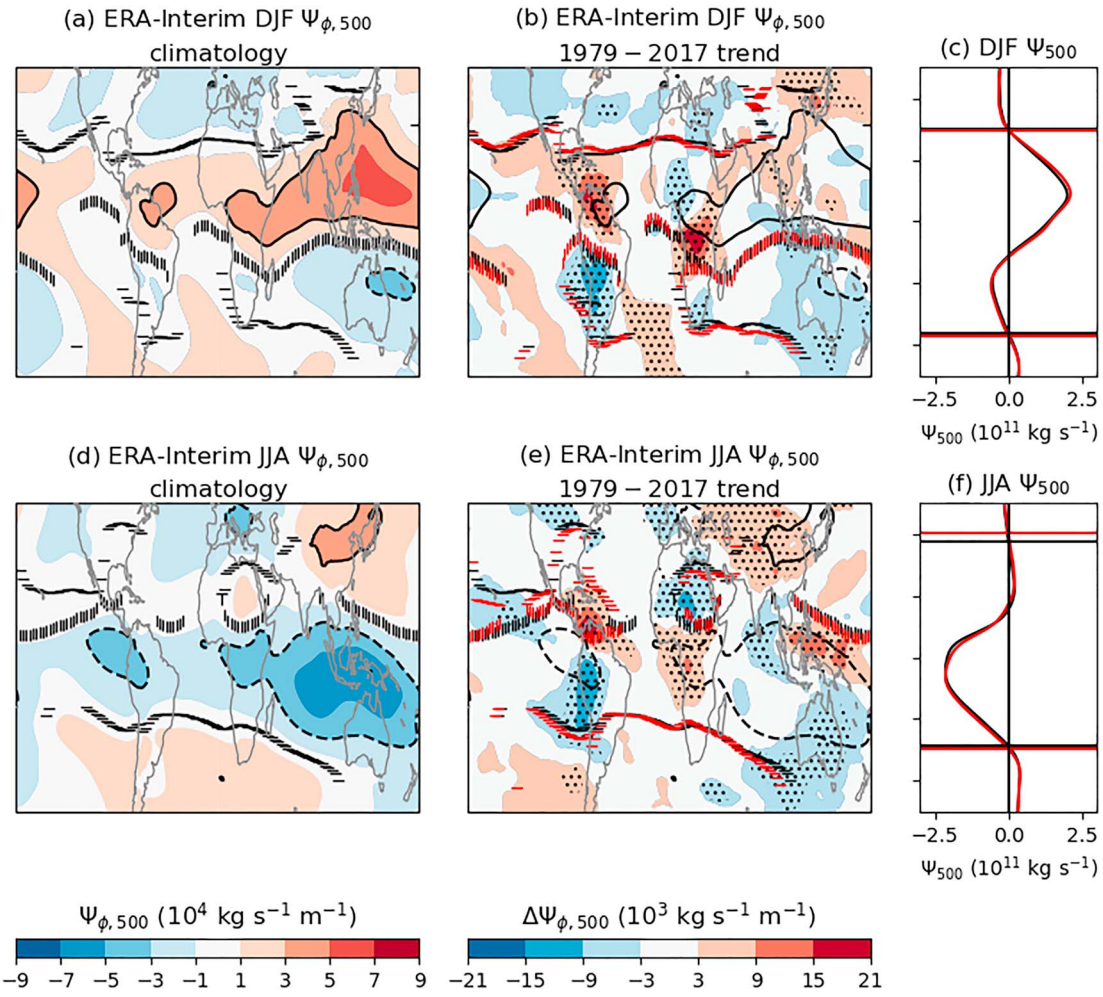

Figure 8. $\Psi_{\phi,500}$ climatology (shaded and contoured in a and d; contoured in b and e) and linear trends (b, e) over the time period 1979–2017 in the ERA-Interim reanalysis during DJF (top row) and JJA (bottom row). The climatological Ψ_{500} (black curve) and the climatology +38-year trend (red curve) are also shown (c, f). Black stippling indicates regions where the least squares fit slope for $\Psi_{\phi,500}$ has a corresponding p value < 0.05. DJF = December–February; JJA = June–August.

3.3. Recent RC Trends in Reanalyses

Given the contrast between the forced and unforced RC anomalies shown in the previous two subsections, we ask the following question: Do recent RC trends in reanalyses more closely resemble unforced variability (section 3.2) or forced changes (section 3.1)? To address this question, we examine trends in $\Psi_{\phi,500}$ and in the RC edge in the ERA-Interim and MERRA2 reanalyses. One important qualification with the results we present in this section is that there is no guarantee that the vertical integral of the zonal mean meridional wind in reanalyses reaches zero at the surface in the mean or in trends (Cheng et al., 2018; Davis et al., 2018; Trenberth, 1991). The stream functions for individual longitudes may similarly contain such artifacts.

In spite of these imperfections of the reanalysis wind field, the RC climatologies from ERA-Interim (Figures 8 and S6) and MERRA2 (Figures S7 and S8) resemble those from models (comparing the contours from Figures 8a and 8d to those in Figures 4a and 4e), although the overturning is slightly stronger in the reanalyses.

The trends in reanalyses over the last 38 years contrast sharply with the multimodel mean forced response (compare Figures 8b, 8c, S6b, and S6c with Figures 4a, 4b, S3a, and S3b). Feng et al. (2015) note that models struggle to capture hemispherically asymmetric trends in general. Here we show that the widening depicted in reanalyses is accompanied by a strengthening of the centers of the RCs, which likewise contrasts with the modeled forced response. This strengthening is stronger in the RC (Figures 8b and S6b

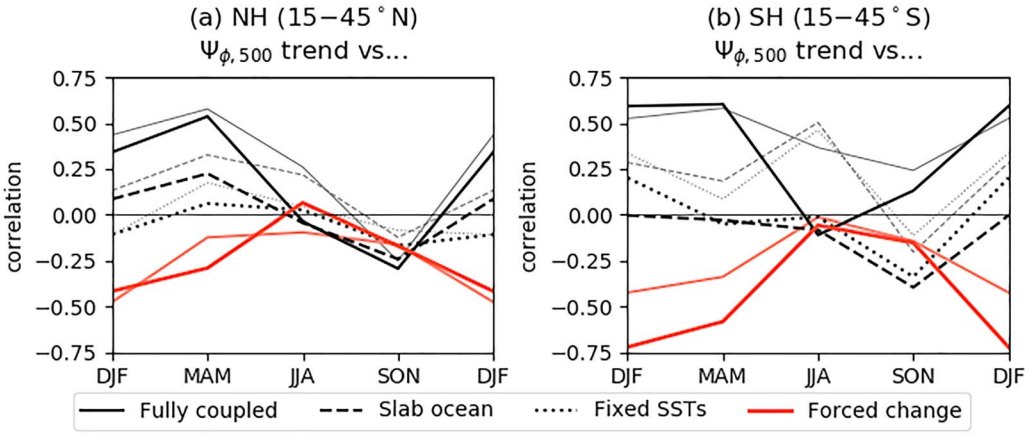

Figure 9. Spatial correlations between the reanalysis $\Psi_{\phi,500}$ trend patterns over (a) 15–45 °N and (b) 15–45 °S with the anomaly pattern from the experiment shown. Black and dark gray curves show the correlation for each season between the Modern-Era Retrospective Analysis for Research and Applications, version 2 (black) and ERA-Interim (gray) trends and unforced anomalies associated with a 2° poleward shift in each hemisphere. The red and salmon curves show the correlation between the MERRA2 (red) and ERA-Interim (salmon) trends and the CMIP5 mean response in $4 \times CO_2$ experiments. DJF = December–February; MAM = March–May; JJA = June–August; SON = September–November; NH = Northern Hemisphere; SH = Southern Hemisphere.

vs. Figures 4a and S3a), than in the HC (Figures 8c, 8f, S6c, and S6f vs. Figures 4b, 4f, S3b, and S3f), owing to opposing intensification at longitudes where the climatological circulation is thermally indirect (e.g., the Eastern South Pacific and South Atlantic). Note that the strengthening is particularly strong over the America's year round.

Reanalysis-based trends in $\Psi_{\phi,500}$ and RC width more closely resemble those due to unforced variability in HC width (compare Figures 8b, 8e, S6b, and S6e with Figures 5, 6, S4, and S5); for example, the NH widening over the Eastern Pacific during DJF (Figures 5a–5c) and the SH widening over the Eastern Pacific during JJA (Figures 6a–6c) also occur in the reanalysis-based trends in the corresponding seasons (Figures 8b and 8e). Correlating the spatial $\Psi_{\phi,500}$ trend pattern between 15° and 45° over each hemisphere with the unforced anomalies and the forced CMIP5 response (Figure 9) suggests that during DJF and MAM not only do trends agree better with unforced widening, but they are actually anticorrelated with the forced response due to greenhouse gas increases.

Recently, increasing evidence has pointed to a substantial role played by natural variability in the widening the tropics (Alfaro-Sánchez et al., 2018; D'Agostino & Lionello, 2017), particularly over recent decades (see the review by Staten et al., 2018; also, Allen & Kovilakam, 2017; Amaya et al., 2017; Grise et al., 2018; Simpson, 2018). This examination of the patterns of RC intensification, weakening, and widening leaves us to conclude that natural variability has also played a decisive role in regional meridional overturning trends as well, but the forced responses to individual forcings, including greenhouse gas increases, stratospheric ozone depletion, and anthropogenic aerosols on $\Psi_{\phi,500}$, and the RC should also be examined and compared to the reanalysis trend, particularly during NH SON, when neither the forced response to CO_2 nor interannual variability associated with HC variations from year to year in CESM can explain the pattern of the observed trend (see also Grise et al., 2018).

The climatology and trends in the RC edge are distinct from those of the upper tropospheric jets (Manney & Hegglin, 2018; hereafter MH18). That said, the latitude and strength of the jets are related to the *intensity* of the RC; the jets have a stronger subtropical component ("radiative component" in MH18) at longitudes where the RC is stronger; this applies to both hemispheres and all seasons (compare Figures 8 and S6 in the present work to panel a of Figures 1–4 of MH18). The edges of the RC parallel the jets over each winter hemisphere and to some extent during the equinoctial seasons, but recent changes in the RC width during DJF are much more regional and varied than the nearly global poleward shift in the jets during DJF. Furthermore, longitudes where the RC strengthens or weakens notably do not show consistent, corresponding shifts in the subtropical jet, in spite of the climatological relationship. It has recently been shown that the

zonal mean subtropical jet and the HC edge latitudes are poorly correlated from year to year (Davis & Birner, 2017; Staten et al., 2018; Waugh et al., 2018); the gap between the two may be even larger at a regional level.

Trends between the changing RC and in SLP likewise show strong differences. Like their climatological maxima, the trends in SLP similarly are largest over longitudes where the RC is not well defined (compare Figures 8b and 8e with Figure 1 from Choi et al., 2014). Thus, even for two fields with moderate year-to-year correlation, the regional responses of the two highlight notable differences not apparent in the zonal mean.

4. Summary and Conclusions

In this work, we generalize the zonal mean HC as a zonally varying RC, following Schwendike et al. (2014). This generalization links the tropical overturning to much of the vertical motion in the tropics and subtropics and consequently to major features in the P-E field. Compared to the subtropical centers of high pressure, the RC edge coincides more closely with the dry, subtropical climates typically ascribed to the subsiding branch of the Hadley cell. This suggests that the RC width metric has potential to relate forced widening to hydrological change. RC width can be overinterpreted where overturning is weak (e.g., over the Eastern USA) as can the HC (e.g., over the NH during JJA). But changes in the RC can be used to understand changes in HC extent, as well as the regional signature of widening. Changes that have previously been examined statistically, such as the relationship between sea surface temperatures in the Asian summer monsoon region and HC extent (Feng, Li, Kucharski, et al., 2018; Feng, Li, Jin, Zhao, et al., 2018; Feng, Li, Jin, & Zheng, 2018), can now be examined directly.

The first-order response of the RC to greenhouse gas increases in CMIP5 is a broad, significant weakening. In contrast, the resulting widening response is regional, and dominated by $\Psi_{\phi,500}$ changes over the Eastern Pacific, where an RC is weakly defined, if at all. Thus, care should be taken before assuming that a widening of the HC implies a widening of the RC at any given location. This model result is, however, for just one forcing, and it differs from patterns of both coupled and uncoupled variability. It seems likely that other forcings, such as aerosol concentration changes and ozone depletion, will have distinct fingerprints as well. The weak correlation between the regional pattern of observed trends in the subtropical $\Psi_{\phi,500}$ and either the forced widening or the year-to-year variations during SON (particularly in the NH; Figure 9) suggests that other forcings or modes of variability are likely needed to explain the observed RC change in this season (Grise et al., 2018). Such spatial attribution work is a logical next step, and the RC metric's validity and strong regionality make it well-suited to such an analysis.

Acknowledgments
We thank Gang Chen and three anonymous reviewers for their constructive comments and valuable insights during the preparation of this manuscript. This work was prepared and published as part of work coordinated by the US CLIVAR Working Group on Changing Width of the Tropical Belt Working Group and by the ISSI Changing Width of the Tropical Belt Working Group. The author was funded by NSF award number 1813981 during the preparation of this manuscript. Computing time and data storage provided by Indiana University's University Information Technology Service. ERA-Interim data are provided by ECMWF and can be obtained in https://www.ecmwf.int/en/forecasts/datasets/reanalysis-datasets/era-interim website. MERRA data are provided by NASA and can be obtained in https://gmao.gsfc.nasa.gov/reanalysis/MERRA-2/data_access/ website. CMIP5 data are hosted at Lawrence Livermore National Laboratory and can be obtained in https://esgf-node.llnl.gov/website. CESM LE data are created and hosted using resources from NSF and CISL and can be obtained in http://www.cesm.ucar.edu/projects/community-projects/LENS/data-sets.html website. Output from this study are archived at the Indiana University Scholarly Data Archive and are available via GLOBUS transfer. Scripts from this study are archived at github.iu.edu and are available upon request.

References

Adam, O., Grise, K. M., Staten, P., Simpson, I. R., Davis, S. M., Davis, N. A., et al. (2018). The TropD software package (v1): Standardized methods for calculating tropical-width diagnostics. *Geoscientific Model Development*, *11*(10), 4339–4357. https://doi.org/10.5194/gmd-11-4339-2018

Alfaro-Sánchez, R., Nguyen, H., Klesse, S., Hudson, A., Belmecheri, S., Köse, N., et al. (2018). Climatic and volcanic forcing of tropical belt northern boundary over the past 800 years. *Nature Geoscience*, *11*(12), 933–938. https://doi.org/10.1038/s41561-018-0242-1

Allen, R. J., & Ajoku, O. (2016). Future aerosol reductions and widening of the northern tropical belt. *Journal of Geophysical Research: Atmospheres*, *121*, 6765–6786. https://doi.org/10.1002/2016JD024803

Allen, R. J., & Kovilakam, M. (2017). The role of natural climate variability in recent tropical expansion. *Journal of Climate*, *30*(16), 6329–6350. https://doi.org/10.1175/JCLI-D-16-0735.1

Allen, R. J., Sherwood, S. C., Norris, J. R., & Zender, C. S. (2012). Recent Northern Hemisphere tropical expansion primarily driven by black carbon and tropospheric ozone. *Nature*, *485*(7398), 350–354. Retrieved from https://doi.org/10.1038/nature11097

Amaya, D. J., Siler, N., Xie, S.-P., & Miller, A. J. (2017). The interplay of internal and forced modes of Hadley Cell expansion: Lessons from the global warming hiatus. *Climate Dynamics*, *51*(1-2), 305–319. https://doi.org/10.1007/s00382-017-3921-5

Angell, J. K., Korshover, J., & Cotten, G. F. (1969). Quasi-biennial variations in the "Centers of Action.". *Monthly Weather Review*, *97*(12), 867–872. https://doi.org/10.1175/1520-0493(1969)097<0867:QVITOA>2.3.CO;2

Betts, A. K. (1998). Climate-convection feedbacks: Some further issues. *Climatic Change*, *39*(1), 35–38. https://doi.org/10.1023/A:1005323805826

Bosilovich, M. G., Akella, S., Coy, L., Cullather, R., Draper, C., Gelaro, R., et al. (2015). MERRA-2: Initial evaluation of the climate.

Ceppi, P., Zappa, G., Shepherd, T. G., & Gregory, J. M. (2018). Fast and slow components of the extratropical atmospheric circulation response to CO_2 forcing. *Journal of Climate*, *31*(3), 1091–1105. https://doi.org/10.1175/JCLI-D-17-0323.1

Chang, E. K. M. (1995). The influence of Hadley circulation intensity changes on extratropical climate in an idealized model. *Journal of the Atmospheric Sciences*, *52*(11), 2006–2024. https://doi.org/10.1175/1520-0469(1995)052<2006:TIOHCI>2.0.CO;2

Chen, G., Lu, J., & Frierson, D. M. W. (2008). Phase speed spectra and the latitude of surface westerlies: Interannual variability and global warming trend. *Journal of Climate*, *21*(22), 5942–5959. https://doi.org/10.1175/2008JCLI2306.1

Chen, S., Wei, K., Chen, W., & Song, L. (2014). Regional changes in the annual mean Hadley circulation in recent decades. *Journal of Geophysical Research: Atmospheres*, *119*, 7815–7832. https://doi.org/10.1002/2014JD021540

Cheng, J., Xu, Z., Hu, P., Hou, X., Gao, C., Hu, S., & Feng, G. (2018). Significant role of orography in shaping the northern hadley circulation and its poleward expansion during boreal summer. *Geophysical Research Letters*, *45*(13), 6619–6627. https://doi.org/10.1029/2018GL079039

Choi, J., Son, S.-W., Lu, J., & Min, S.-K. (2014). Further observational evidence of Hadley cell widening in the Southern Hemisphere. *Geophysical Research Letters*, *41*, 2590–2597. https://doi.org/10.1002/2014GL059426

Cook, B. I., Smerdon, J. E., Seager, R., & Coats, S. (2014). Global warming and 21st century drying. *Climate Dynamics*, *43*(9-10), 2607–2627. https://doi.org/10.1007/s00382-014-2075-y

D'Agostino, R., & Lionello, P. (2017). Evidence of global warming impact on the evolution of the Hadley Circulation in ECMWF centennial reanalyses. *Climate Dynamics*, *48*(9-10), 3047–3060. https://doi.org/10.1007/s00382-016-3250-0

D'Agostino, R., Lionello, P., Adam, O., & Schneider, T. (2017). Factors controlling Hadley circulation changes from the Last Glacial Maximum to the end of the 21st century. *Geophysical Research Letters*, *44*, 8585–8591. https://doi.org/10.1002/2017GL074533

Davis, N., & Birner, T. (2017). On the Discrepancies in tropical belt expansion between reanalyses and climate models and among tropical belt width metrics. *Journal of Climate*, *30*(4), 1211–1231. https://doi.org/10.1175/JCLI-D-16-0371.1

Davis, N. A., Davis, S. M., & Waugh, D. W. (2018). New insights into tropical belt metrics. *US CLIVAR Variations*, *16*(2), 1–7. https://doi.org/10.5065/D69Z93QF

Davis, N. A., Seidel, D. J., Birner, T., Davis, S. M., & Tilmes, S. (2016). Changes in the width of the tropical belt due to simple radiative forcing changes in the GeoMIP simulations. *Atmospheric Chemistry and Physics*, *16*(15), 10,083–10,095. https://doi.org/10.5194/acp-16-10083-2016

Davis, S. M., & Rosenlof, K. H. (2012). A multidiagnostic intercomparison of tropical-width time series using reanalyses and satellite observations. *Journal of Climate*, *25*(4), 1061–1078. https://doi.org/10.1175/JCLI-D-11-00127.1

Dee, D. P., Uppala, S. M., Simmons, A. J., Berrisford, P., Poli, P., Kobayashi, S., et al. (2011). The ERA-Interim reanalysis: Configuration and performance of the data assimilation system. *Quarterly Journal of the Royal Meteorological Society*, *137*(656), 553–597. https://doi.org/10.1002/qj.828

Doxsey-Whitfield, E., MacManus, K., Adamo, S. B., Pistolesi, L., Squires, J., Borkovska, O., & Baptista, S. R. (2015). Taking advantage of the improved availability of census data: A first look at the gridded population of the world, Version 4. *Papers in Applied Geography*, *1*(3), 226–234. https://doi.org/10.1080/23754931.2015.1014272

Feldl, N., & Bordoni, S. (2015). Characterizing the Hadley circulation response through regional climate feedbacks. *Journal of Climate*, *29*(2), 613–622. https://doi.org/10.1175/JCLI-D-15-0424.1

Feng, J., Li, J., Jin, F., Zhao, S., & Zhu, J. (2018). Relationship between the Hadley circulation and different tropical meridional SST structures during boreal summer. *Journal of Climate*, *31*(16), 6575–6590. https://doi.org/10.1175/JCLI-D-18-0095.1

Feng, J., Li, J., Jin, F.-F., & Zheng, F. (2018). A comparison of the response of the Hadley circulation to different tropical SST meridional structures during the equinox seasons. *Journal of Geophysical Research: Atmospheres*, *123*(5), 2591–2604. https://doi.org/10.1002/2017JD028219

Feng, J., Li, J., Kucharski, F., Wang, Y., Sun, C., Xie, F., & Yang, Y. (2018). Modulation of the meridional structures of the Indo-Pacific warm pool on the response of the Hadley circulation to tropical SST. *Journal of Climate*, *31*(21), 8971–8984. https://doi.org/10.1175/JCLI-D-18-0305.1

Feng, J., Li, J., & Xie, F. (2012). Long-term variation of the principal mode of boreal spring Hadley circulation linked to SST over the Indo-Pacific warm pool. *Journal of Climate*, *26*(2), 532–544. https://doi.org/10.1175/JCLI-D-12-00066.1

Feng, J., Li, J., Zhu, J., Li, F., & Sun, C. (2015). Simulation of the equatorially asymmetric mode of the Hadley circulation in CMIP5 models. *Advances in Atmospheric Sciences*, *32*(8), 1129–1142. https://doi.org/10.1007/s00376-015-4157-0

Freitas, A. C. V., Aímola, L., Ambrizzi, T., & de Oliveira, C. P. (2017). Extreme intertropical convergence zone shifts over southern maritime continent. *Atmospheric Science Letters*, *18*(1), 2–10. https://doi.org/10.1002/asl.716

Fu, Q., Johanson, C. M., Wallace, J. M., & Reichler, T. (2006). Enhanced mid-latitude tropospheric warming in satellite measurements. *Science*, *312*(5777), 1179. https://doi.org/10.1126/science.1125566

Garfinkel, C. I., Waugh, D. W., & Polvani, L. M. (2015). Recent Hadley cell expansion: The role of internal atmospheric variability in reconciling modeled and observed trends. *Geophysical Research Letters*, *42*, 10,824–10,831. https://doi.org/10.1002/2015GL066942

Gelaro, R., McCarty, W., Suárez, M. J., Todling, R., Molod, A., Takacs, L., et al. (2017). The Modern-Era Retrospective Analysis for Research and Applications, version 2 (MERRA-2). *Journal of Climate*, *30*(14), 5419–5454. https://doi.org/10.1175/JCLI-D-16-0758.1

Grassi, B., Redaelli, G., Canziani, P. O., & Visconti, G. (2011). Effects of the PDO phase on the tropical belt width. *Journal of Climate*, *25*(9), 3282–3290. https://doi.org/10.1175/JCLI-D-11-00244.1

Grise, K. M., Davis, S. M., Simpson, I. R., Waugh, D. W., Fu, Q., Allen, R. J., et al. (2019). Recent tropical expansion: Natural variability or forced response? *Journal of Climate*, *32*(5), 1551–1571. https://doi.org/10.1175/JCLI-D-18-0444.1

Grise, K. M., Davis, S. M., & Staten, P. W. (2018). Regional and seasonal characteristics of the recent expansion of the tropics. *Journal of Climate*, *31*(17), 6839–6856. https://doi.org/10.1175/JCLI-D-18-0060.1

Grise, K. M., & Polvani, L. M. (2014). The response of midlatitude jets to increased CO_2: Distinguishing the roles of sea surface temperature and direct radiative forcing. *Geophysical Research Letters*, *41*, 6863–6871. https://doi.org/10.1002/2014GL061638

Grise, K. M., & Polvani, L. M. (2016). Is climate sensitivity related to dynamical sensitivity? *Journal of Geophysical Research: Atmospheres*, *121*, 5159–5176. https://doi.org/10.1002/2015JD024687

Grise, K. M., & Polvani, L. M. (2017). Understanding the time scales of the tropospheric circulation response to abrupt CO_2 forcing in the Southern Hemisphere: Seasonality and the role of the stratosphere. *Journal of Climate*, *30*(21), 8497–8515. https://doi.org/10.1175/JCLI-D-16-0849.1

Guo, Y., Li, J., Feng, J., Xie, F., Sun, C., & Zheng, J. (2016). The multidecadal variability of the asymmetric mode of the boreal autumn Hadley circulation and its link to the Atlantic multidecadal oscillation. *Journal of Climate*, *29*(15), 5625–5641. https://doi.org/10.1175/JCLI-D-15-0025.1

Held, I. M., & Soden, B. J. (2006). robust responses of the hydrological cycle to global warming. *Journal of Climate*, *19*(21), 5686–5699. https://doi.org/10.1175/JCLI3990.1

Hoskins, B. (1996). On the existence and strength of the summer subtropical anticyclones. *Bulletin of the American Meteorological Society*, *77*(6), 1279–1292. https://doi.org/10.1175/1520-0477-77.6.1279

Hu, S., Cheng, J., & Chou, J. (2017). Novel three-pattern decomposition of global atmospheric circulation: Generalization of traditional two-dimensional decomposition. *Climate Dynamics*, *49*(9-10), 3573–3586. https://doi.org/10.1007/s00382-017-3530-3

Hu, Y., & Fu, Q. (2007). Observed poleward expansion of the Hadley circulation since 1979. *Atmospheric Chemistry and Physics*, *7*(19), 5229–5236. https://doi.org/10.5194/acp-7-5229-2007

Huang, R., Chen, S., Chen, W., & Hu, P. (2018). Interannual variability of regional Hadley circulation intensity over Western Pacific during boreal winter and its climatic impact over Asia-Australia region. *Journal of Geophysical Research: Atmospheres*, *123*(1), 344–366. https://doi.org/10.1002/2017JD027919

Kang, S. M., Deser, C., & Polvani, L. M. (2013). Uncertainty in climate change projections of the Hadley circulation: The role of internal variability. *Journal of Climate*, *26*(19), 7541–7554. https://doi.org/10.1175/JCLI-D-12-00788.1

Kang, S. M., Held, I. M., Frierson, D. M. W., & Zhao, M. (2008). The response of the ITCZ to extratropical thermal forcing: Idealized slab-ocean experiments with a GCM. *Journal of Climate*, *21*(14), 3521–3532. https://doi.org/10.1175/2007JCLI2146.1

Karnauskas, K. B., Donnelly, J. P., & Anchukaitis, K. J. (2016). Future freshwater stress for island populations. *Nature Climate Change*, *6*(7), 720–725. https://doi.org/10.1038/nclimate2987

Karnauskas, K. B., Schleussner, C.-F., Donnelly, J. P., & Anchukaitis, K. J. (2018). Freshwater stress on small island developing states: population projections and aridity changes at 1.5 and 2 °C. *Regional Environmental Change*, *18*(8), 2273–2282. https://doi.org/10.1007/s10113-018-1331-9

Karnauskas, K. B., & Ummenhofer, C. C. (2014). On the dynamics of the Hadley circulation and subtropical drying. *Climate Dynamics*, *42*(9-10), 2259–2269. https://doi.org/10.1007/s00382-014-2129-1

Kay, J. E., Deser, C., Phillips, A., Mai, A., Hannay, C., Strand, G., et al. (2014). The Community Earth System Model (CESM) Large Ensemble project: A community resource for studying climate change in the presence of internal climate variability. *Bulletin of the American Meteorological Society*, *96*(8), 1333–1349. https://doi.org/10.1175/BAMS-D-13-00255.1

Keyser, D., Schmidt, B. D., & Duffy, D. G. (1989). A technique for representing three-dimensional vertical circulations in baroclinic disturbances. *Monthly Weather Review*, *117*(11), 2463–2494. https://doi.org/10.1175/1520-0493(1989)117<2463:ATFRTD>2.0.CO;2

Kim, Y.-H., Min, S.-K., Son, S.-W., & Choi, J. (2017). Attribution of the local Hadley cell widening in the Southern Hemisphere. *Geophysical Research Letters*, *44*, 1015–1024. https://doi.org/10.1002/2016GL072353

Kovilakam, M., & Mahajan, S. (2016). Confronting the "Indian summer monsoon response to black carbon aerosol" with the uncertainty in its radiative forcing and beyond. *Journal of Geophysical Research: Atmospheres*, *121*, 7833–7852. https://doi.org/10.1002/2016JD024866

Li, J., Menzel, W. P., Zhang, W., Sun, F., Schmit, T. J., Gurka, J. J., & Weisz, E. (2004). Synergistic use of MODIS and AIRS in a variational retrieval of cloud parameters. *Journal of Applied Meteorology*, *43*(11), 1619–1634. https://doi.org/10.1175/JAM2166.1

Lu, J., Chen, G., & Frierson, D. M. W. (2008). Response of the zonal mean atmospheric circulation to El Niño versus global warming. *Journal of Climate*, *21*(22), 5835–5851. https://doi.org/10.1175/2008JCLI2200.1

Lucas, C., & Nguyen, H. (2015). Regional characteristics of tropical expansion and the role of climate variability. *Journal of Geophysical Research: Atmospheres*, *120*, 6809–6824. https://doi.org/10.1002/2015JD023130

Lucas, C., Nguyen, H., & Timbal, B. (2012). An observational analysis of Southern Hemisphere tropical expansion. *Journal of Geophysical Research*, *117*, D17112. https://doi.org/10.1029/2011JD017033

Manney, G. L., & Hegglin, M. I. (2018). Seasonal and regional variations of long-term changes in upper-tropospheric jets from reanalyses. *Journal of Climate*, *31*(1), 423–448. https://doi.org/10.1175/JCLI-D-17-0303.1

Mantsis, D. F., Sherwood, S., Allen, R., & Shi, L. (2017). Natural variations of tropical width and recent trends. *Geophysical Research Letters*, *44*, 3825–3832. https://doi.org/10.1002/2016GL072097

Mathew, S. S., & Kumar, K. K. (2018). Estimation of zonally resolved edges of the tropical belt using GPS-RO measurements. *IEEE Journal of Selected Topics in Applied Earth Observations and Remote Sensing*, *11*(7), 2555–2561. https://doi.org/10.1109/JSTARS.2018.2828342

Mbengue, C., & Schneider, T. (2018). Linking Hadley circulation and storm tracks in a conceptual model of the atmospheric energy balance. *Journal of the Atmospheric Sciences*, *75*(3), 841–856. https://doi.org/10.1175/JAS-D-17-0098.1

McLandress, C., Jonsson, A. I., Plummer, D. A., Reader, M. C., Scinocca, J. F., & Shepherd, T. G. (2010). Separating the dynamical effects of climate change and ozone depletion. Part I: Southern Hemisphere stratosphere. *Journal of Climate*, *23*(18), 5002–5020. https://doi.org/10.1175/2010JCLI3586.1

Min, S., & Son, S. (2013). Multimodel attribution of the Southern Hemisphere Hadley cell widening: Major role of ozone depletion. *Journal of Geophysical Research: Atmospheres*, *118*, 3007–3015. https://doi.org/10.1002/jgrd.50232

Nguyen, H., Evans, A., Lucas, C., Smith, I., & Timbal, B. (2012). The Hadley circulation in reanalyses: Climatology, variability, and change. *Journal of Climate*, *26*(10), 3357–3376. https://doi.org/10.1175/JCLI-D-12-00224.1

Nguyen, H., Hendon, H. H., Lim, E.-P., Boschat, G., Maloney, E., & Timbal, B. (2017). Variability of the extent of the Hadley circulation in the southern hemisphere: A regional perspective. *Climate Dynamics*, *50*(1-2), 129–142. https://doi.org/10.1007/s00382-017-3592-2

Nguyen, H., Lucas, C., Evans, A., Timbal, B., & Hanson, L. (2015). Expansion of the Southern Hemisphere Hadley cell in response to greenhouse gas forcing. *Journal of Climate*, *28*(20), 8067–8077. https://doi.org/10.1175/JCLI-D-15-0139.1

Pena-Ortiz, C., Gallego, D., Ribera, P., Ordonez, P., & Alvarez-Castro, M. D. C. (2013). Observed trends in the global jet stream characteristics during the second half of the 20th century. *Journal of Geophysical Research: Atmospheres*, *118*, 2702–2713. https://doi.org/10.1002/jgrd.50305

Polvani, L. M., Waugh, D. W., Correa, G. J. P., & Son, S.-W. (2010). Stratospheric ozone depletion: The main driver of twentieth-century atmospheric circulation changes in the Southern Hemisphere. *Journal of Climate*, *24*(3), 795–812. https://doi.org/10.1175/2010JCLI3772.1

Quan, X.-W., Hoerling, M. P., Perlwitz, J., Diaz, H. F., & Xu, T. (2014). How fast are the tropics expanding? *Journal of Climate*, *27*(5), 1999–2013. https://doi.org/10.1175/JCLI-D-13-00287.1

Rodwell, M. J., & Hoskins, B. J. (1996). Monsoons and the dynamics of deserts. *Quarterly Journal of the Royal Meteorological Society*, *122*(534), 1385–1404. https://doi.org/10.1002/qj.49712253408

Scheff, J., & Frierson, D. M. W. (2015). Terrestrial aridity and its response to greenhouse warming across CMIP5 climate models. *Journal of Climate*, *28*(14), 5583–5600. https://doi.org/10.1175/JCLI-D-14-00480.1

Schmidt, D. F., & Grise, K. M. (2017). The response of local precipitation and sea level pressure to Hadley cell expansion. *Geophysical Research Letters*, *44*, 10,573–10,582. https://doi.org/10.1002/2017GL075380

Schneider, T., Bischoff, T., & Haug, G. H. (2014). Migrations and dynamics of the intertropical convergence zone. *Nature*, *513*(7516), 45–53. https://doi.org/10.1038/nature13636

Schneider, T., O'Gorman, P. A., & Levine, X. J. (2010). Water vapor and the dynamics of climate changes. *Reviews of Geophysics*, *48*, RG3001. https://doi.org/10.1029/2009RG000302

Schwendike, J., Berry, G. J., Reeder, M. J., Jakob, C., Govekar, P., & Wardle, R. (2015). Trends in the local Hadley and local Walker circulations. *Journal of Geophysical Research: Atmospheres*, *120*, 7599–7618. https://doi.org/10.1002/2014JD022652

Schwendike, J., Govekar, P., Reeder, M. J., Wardle, R., Berry, G. J., & Jakob, C. (2014). Local partitioning of the overturning circulation in the tropics and the connection to the Hadley and Walker circulations. *Journal of Geophysical Research: Atmospheres*, *119*, 1322–1339. https://doi.org/10.1002/2013JD020742

Seager, R., Harnik, N., Kushnir, Y., Robinson, W., & Miller, J. (2003). Mechanisms of hemispherically symmetric climate variability. *Journal of Climate*, *16*(18), 2960–2978. https://doi.org/10.1175/1520-0442(2003)016<2960:MOHSCV>2.0.CO;2

Seager, R., Naik, N., & Vecchi, G. A. (2010). Thermodynamic and dynamic mechanisms for large-scale changes in the hydrological cycle in response to global warming. *Journal of Climate*, *23*(17), 4651–4668. https://doi.org/10.1175/2010JCLI3655.1

Seidel, D. J., Fu, Q., Randel, W. J., & Reichler, T. J. (2008). Widening of the tropical belt in a changing climate. *Nature Geoscience*, *1*(1), 21–24. https://doi.org/10.1038/ngeo.2007.38

Seidel, D. J., & Randel, W. J. (2007). Recent widening of the tropical belt: Evidence from tropopause observations. *Journal of Geophysical Research*, *112*, D20113. https://doi.org/10.1029/2007JD008861

Shaw, T. A., & Voigt, A. (2016). What can moist thermodynamics tell us about circulation shifts in response to uniform warming? *Geophysical Research Letters*, *43*, 4566–4575. https://doi.org/10.1002/2016GL068712

Simpson, I. R. (2018). Natural variability in the width of the tropics. *US CLIVAR Variations*, *16*(2), 14–20. https://doi.org/10.5065/D69Z93QF

Simpson, I. R., Shaw, T. A., & Seager, R. (2014). A diagnosis of the seasonally and longitudinally varying midlatitude circulation response to global warming. *Journal of the Atmospheric Sciences*, *71*(7), 2489–2515. https://doi.org/10.1175/JAS-D-13-0325.1

Son, S.-W., Gerber, E. P., Perlwitz, J., Polvani, L. M., Gillett, N. P., Seo, K.-H., et al. (2010). Impact of stratospheric ozone on Southern Hemisphere circulation change: A multimodel assessment. *Journal of Geophysical Research*, *115*, D00M07. https://doi.org/10.1029/2010JD014271

Song, F., Leung, L. R., Lu, J., & Dong, L. (2018). Future changes in seasonality of the North Pacific and North Atlantic subtropical highs. *Geophysical Research Letters*, *45*(21), 11,959–11,968. https://doi.org/10.1029/2018GL079940

Stanfield, R. E., Jiang, J. H., Dong, X., Xi, B., Su, H., Donner, L., et al. (2016). A quantitative assessment of precipitation associated with the ITCZ in the CMIP5 GCM simulations. *Climate Dynamics*, *47*(5-6), 1863–1880. https://doi.org/10.1007/s00382-015-2937-y

Staten, P. W., Lu, J., Grise, K. M., Davis, S. M., & Birner, T. (2018). Re-examining tropical expansion. *Nature Climate Change*, *8*(9), 768–775. https://doi.org/10.1038/s41558-018-0246-2

Staten, P. W., Reichler, T., & Lu, J. (2014). The transient circulation response to radiative forcings and sea surface warming. *Journal of Climate*, *27*(24), 9323–9336. https://doi.org/10.1175/JCLI-D-14-00035.1

Staten, P. W., Rutz, J. J., Reichler, T., & Lu, J. (2012). Breaking down the tropospheric circulation response by forcing. *Climate Dynamics*, *39*(9–10), 2361–2375. https://doi.org/10.1007/s00382-011-1267-y

Stocker, T. F., Qin, D., Plattner, G.-K., Tignor, M. B., Allen, S., Boschung, J., et al. (2013). *IPCC, 2013: Summary for policymakers*. Cambridge, UK and New York: Cambridge University Press.

Taylor, K. E., Stouffer, R. J., & Meehl, G. A. (2011). An overview of CMIP5 and the experiment design. *Bulletin of the American Meteorological Society*, *93*(4), 485–498. https://doi.org/10.1175/BAMS-D-11-00094.1

Totz, S., Petri, S., Lehmann, J., & Coumou, D. (2018). Regional changes in the mean position and variability of the tropical edge. *Geophysical Research Letters*, *45*(21), 12,076–12,084. https://doi.org/10.1029/2018GL079911

Trenberth, K. E. (1991). Climate diagnostics from global analyses: Conservation of mass in ECMWF analyses. *Journal of Climate*, *4*(7), 707–722. https://doi.org/10.1175/1520-0442(1991)004<0707:CDFGAC>2.0.CO;2

Vecchi, G. A., & Soden, B. J. (2007). Increased tropical Atlantic wind shear in model projections of global warming. *Geophysical Research Letters*, *34*, L08702. https://doi.org/10.1029/2006GL028905

Waugh, D. W., Grise, K. M., Seviour, W., Davis, S. M., Davis, N., Adam, O., et al. (2018). Revisiting the relationship among metrics of tropical expansion. *Journal of Climate*, *31*, 7565–7581. https://doi.org/10.1175/JCLI-D-18-0108.1

Zhao, H., & Moore, G. W. K. (2008). Trends in the boreal summer regional Hadley and Walker circulations as expressed in precipitation records from Asia and Africa during the latter half of the 20th century. *International Journal of Climatology*, *28*, 563–578. https://doi.org/10.1002/joc.1580